SAND2008-2875P

Uncertainty Quantification for the Simple Prototype Analysis

Brian Rutherford, Joe Castro, Vicente Romero and Rob Hoekstra

4/16/08

Prepared by
Sandia National Laboratories
Albuquerque, New Mexico 87185 and Livermore, California 94550
Sandia is a multiprogram laboratory operated by Sandia Corporation,
a Lockheed Martin Company, for the United States Department of Energy's
National Nuclear Security Administration under Contract DE-AC04-94-AL85000.

I Introduction.

The purpose of this report is to provide details of the uncertainty quantification, bias characterization and accommodation, and extrapolation processes used in the QASPR simple prototype analysis. We discuss the processes used to calibrate, "normalize" and characterize uncertainty for the system prior to comparing results with the SPR prototype data. We also consider how this quantification of uncertainty would be used by the system for further prediction. The procedures involved are outlined in the body of the report with the some of the technical details deferred to appendices.

In the remainder of this section, we discuss issues that influenced the approach taken. The subsection, "Prediction Requirements" addresses inferences (not necessarily unique to the QASPR process) that are often required of computational analyses in an engineering environment. We argue that to make these inferences, a number of components of "total uncertainty" -- variability and epistemic uncertainty (epistemic uncertainty is referred to as "uncertainty" in the remainder of this report) require separate characterization. The next two subsections, "Limitations in the Experimental Data" and "Facility and Device Bias Estimation" provide part of the motivation for the specific methods used for the QASPR simple prototype analysis.

The three remaining sections and the appendices give more detail on the approach. Section II, "Variability and Uncertainty Assessment", contains three subsections detailing the characterization of device variability, device uncertainty and facility uncertainty respectively, using the experimental data. Section III, "Calibration and Bias Estimation", describes procedures unique to the QASPR project where inferences based on experimental data at different facilities and for different devices are incorporated into the computational system where they can be utilized for prediction. Separate subsections address analyses of SPR model development data, ACRR model development data and ACRR prototype data. The final section, "Model-Based Prediction", describes how the computational responses are generated for comparison with the SPR prototype data and how responses would be generated in more general predictive scenarios.

Prediction Requirements

As the QASPR Program develops it is anticipated that the inferences requested of the project will be substantial. It is common in large-scale computational applications that both a predicted response and a prediction of the range of responses are required. These inferences are needed in validation (for comparison with experimental results) and in prediction (to characterize the mean and range of expected performance). In addition, it is common in these applications and likely for the QASPR project that "prediction bounds" and/or "tolerance bounds" will be requested. These bounds and the methods required for their calculation are discussed in the following paragraphs.

In order to meet the prediction requirements anticipated for the QASPR program, it is important to characterize and maintain separately, several quantities related to total uncertainty. Separate treatment of (a) facility uncertainty, (b) device variability and (c) device uncertainty are discussed in this subsection. Experimental response values are compared to computational predictions to help characterize these quantities and to assess the models predictive capabilities. We use the following definitions in the simple prototype exercise.

a) Facility uncertainty -- differences in device response due to uncertainty in boundary conditions provided for the experimental shots. Fluence magnitude is the boundary condition with the largest impact. Differences between the target and actual fluence levels are measured and the associated device responses are normalized to adjust for these differences. Errors in these measurements, however, result in errors in fluence level used for the normalization process. Facility uncertainty refers to the shot-to-shot differences that result from these normalization errors.
b) Device variability -- differences in device responses that result from physical and material variations between devices. These are assumed to be a consequence of variation in manufacturing process.
c) Device uncertainty -- uncertainty in the device mean performance. Device uncertainty is a consequence of the limited number of experiments upon which the means are calculated.

In the remainder of this subsection, we describe several types of inferences that are likely to be required of the QASPR process. Two hypothetical examples are given next to help illustrate the concepts. In these examples it is assumed (for simplicity of the illustration) that the uncertainty applies only to the "location" of the distribution characterizing device variability (i.e. there is uncertainty in the mean value of the response distribution, but not otherwise in its form). In many computational modeling situations the limited data don't permit much further sophistication.

In the first example, we consider how estimated uncertainty and estimated variability can be used in making inferences. Consider the two hypothetical predictive situations indicated in Figure 1. The blue density function $g(r)$ on the left characterizes uncertainty for this hypothetical example. The green density function $f(r)$ on the right captures variability in the response. The red density function $h(r)$ on the right, is constructed to model their combined uncertainty and is computed as the convolution of $f(r)$ and $g(r)$.

So the density functions represent:

$g(r)$ – uncertainty;
$f(r)$ – variability; and
$h(r) = f(r) \circ g(r)$ -- uncertainty and variability combined.

Percentiles taken from $h(r)$ provide "prediction bounds" for the response. The prediction bounds can be used to obtain, for example, the response value r^* below which $ZZ\%$ of future responses generated under similar conditions should fall (see Figure 1a). The

prediction bounds take into account the range of the responses as well as uncertainty in the modeling.

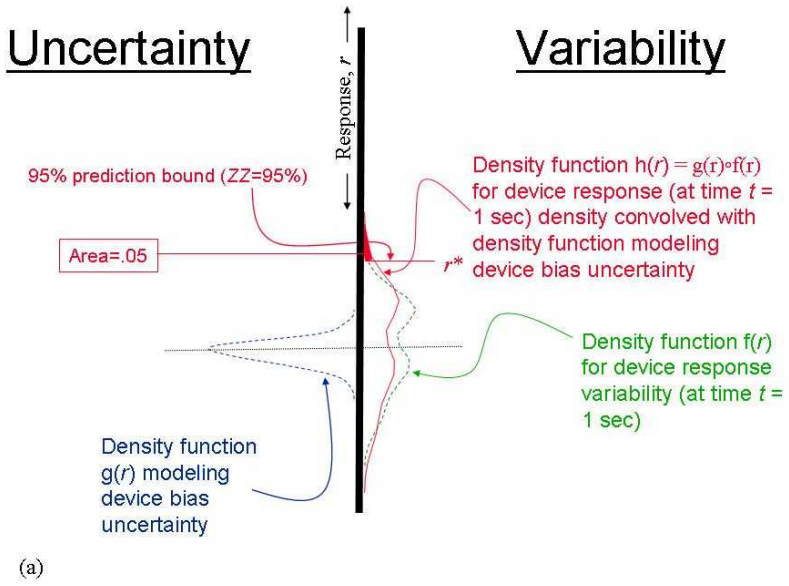

Figure 1a. Constructing Prediction Bounds. Figure 1a illustrates how uncertainty and variability can be combined to compute prediction bounds.

In the QASPR simple prototype analysis uncertainty that is a consequence of data limitations and measurement errors is incorporated into the Charon model parameters. Prediction bounds are constructed through Charon runs simulating the SPR prototype responses. These responses are compared with the SPR Fairchild data to provide an indication of QASPR system performance. If the system were performing "perfectly" (i.e. generating responses distributed identically to the experimental process) we would "expect" *ZZ* percent of the experimental results to fall within the bounds (on average over repeated application).

Another question often asked in an engineering environment calls for "tolerance bounds" for the response. Tolerance bounds address the confidence statement: "we are *XX* percent confident that *YY* percent of the responses will fall below the threshold *r***". To compute this threshold, one would use the blue and green densities as indicated in Figure 1b. The mean value for the density $f(r)$ is established at the XX^{th} percentile of $g(r)$ and the tolerance bound *r*** is then taken as the YY^{th} percentile of $f(r)$. We don't make use of tolerance bounds in this report. The point of this illustration is to show that in order to eventually make these types of inference, it is necessary to establish a framework maintaining the appropriate distinctions in characterization of total uncertainty.

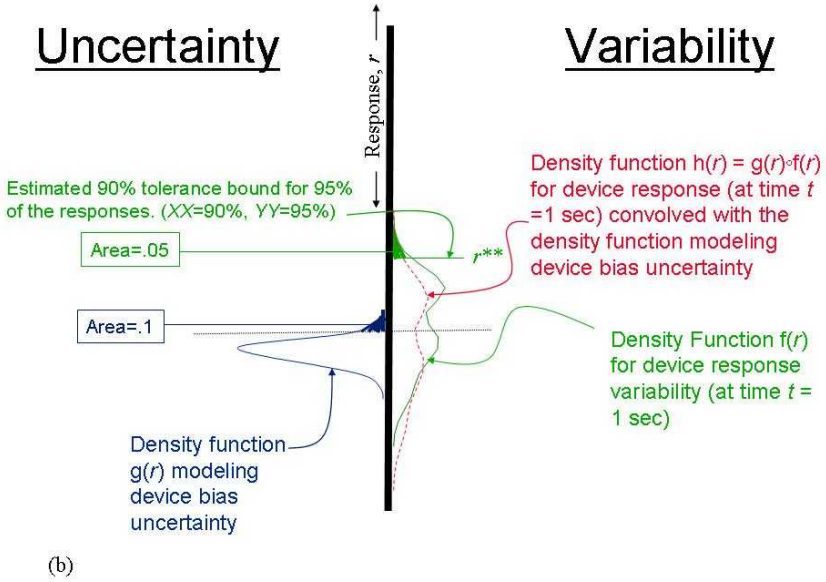

Figure 1b. Constructing Tolerance Bounds. Figure 1b illustrates how uncertainty and variability can be used to compute tolerance bounds.

We should note here that using density functions to represent the uncertainty in this hypothetical example was done strictly for ease of explanation. In many situations this uncertainty would be more realistically accommodated through the use of probabilistic bounds or characterized through non-probabilistic methods, such as uncertainty intervals. In these situations, the analysis could be more complicated because of the procedures needed to make inferences combining methodologies. However, it would still be necessary to maintain the distinctions between uncertainty and variability, as suggested above, to make the required inferences.

In this second example, we consider the uses of the device and facility components of total uncertainty. The variability and uncertainty associated with the device should be accounted for in any predictive setting, while some components of facility uncertainty apply only to analyses at a specific facility. Figure 2 illustrates this concern. The red density function on the right is assumed to model the combination of device variability and uncertainty and facility uncertainty. Percentiles from this density function should be used to compare the model predictions to the experimental data at the facility where the uncertainty was estimated, but it would not necessarily be appropriate to use these percentiles to predict the range of device performance at other facilities or where specific boundary conditions have been provided. Only part of the facility uncertainty carries forward to more general predictions. In the QASPR simple prototype setting, the variance in response that is a consequence of errors in the fluence measurements only affects the general prediction uncertainty to the extent that it contributes to uncertainty in the mean inverse gain for a device and facility. Only a small portion of the facility uncertainty applies to prediction in the more general setting.

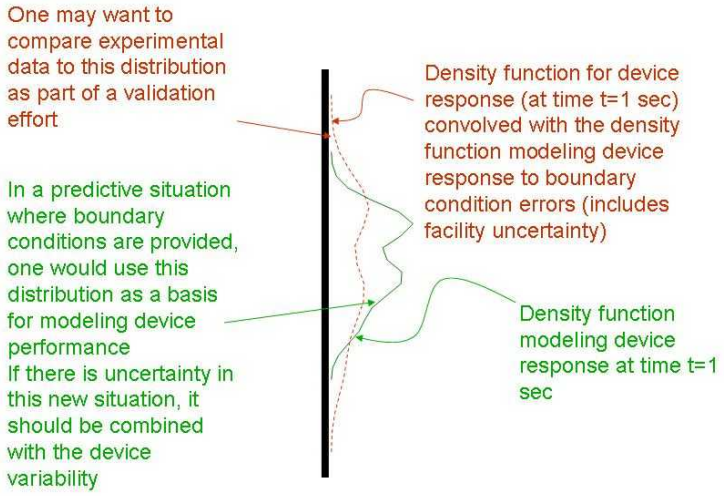

Figure 2. Separate Assessment of Facility Uncertainty and Device Variability.

Figures 1 and 2, together with the associated discussion suggest that we separately establish and quantify facility uncertainty, device variability and device uncertainty. In the "Variability and Uncertainty Assessment" Section, we describe methods involved in characterization of these three quantities in more detail for the experimental data. These quantities should be compared to the corresponding partitioning of total uncertainty on the computational side as part of a validation procedures involved in the SPR simple prototype analysis.

Limitations in the Experimental Data

One motivating factor for our use of the pre-rad data in modeling the components of total uncertainty was the paucity of data. Table 1 lists summary statistics for the data considered in this analysis. Five data sets or "experimental series", were analyzed with the sixth series (SPR prototype) to be predicted. These five experimental series are:

SPR	model development devices -- SPR cavity shots, Microsemi diffusion lot #1 data;
ACRR (high)	model development devices -- ACRR high fluence shots, Microsemi diffusion lot #1 data;
ACRR (high)	prototype devices -- ACRR high fluence shots, Fairchild data;
ACRR (low)	model development devices -- ACRR low fluence shots, Microsemi diffusion lot #1 data; and
ACRR (low)	prototype devices -- ACRR low fluence shots, Fairchild data.

There were only a limited number of experimental shots (six SPR Microsemi shots with a total of 17 devices and three ACRR (high fluence) shots with a total of 18 devices for the model development and prototype shot series) providing the basis for calibration and

estimation of the device bias. Table 1 gives statistics based on the inverse gain values at time, $t = 1$ sec.

Because of the small number of shots and devices in each experimental series, these estimates are imprecise; the precision is indicated by the two standard error bounds given in the columns adjacent to the estimate. The factor of two difference between upper and lower bounds (that define an approximate 95% confidence interval) in the device standard deviation is of particular concern because these estimates are used to establish the range of device performance in any predictive scenario.

Table 1. Standard Deviation Table for Facility Uncertainty and Device Variability. The results marked with a "*" are based on the weighted average of the device responses to reflect the number of devices associated with each shot. The omitted bounds marked instead with "**" come from unbalanced designs were reliable methods for constructing the bounds are not available for small data sets. The 95% bounds shown are computed using method of moments estimates (see "Analysis of Messy Data, Volume I: Designed Experiments", Milliken and Johnson (1992) pages 255 -- 262).

Facility/Device	Number of Shots	Number of Devices	**Mean Inverse Gain**	Lower bound	**Facility Standard Deviation**	Upper bound	Lower bound	**Device Standard Deviation**	Upper bound
ACRR (high fluence) Prototype	3	18	1.58	0	.014	.159	.039	.053	.082
SPR Model Development	6	14	1.46 *	**	0	**	.058	.081	.130
ACRR (high fluence) Model Development	3	18	1.13	0	0	.223	.074	.091	.118
ACRR (lower fluence) Prototype	5	21	*	**		**	**		**
ACRR (lower fluence) Model Development	3	6							

The limitation on the number of experimental data is only part of the difficulty in characterization of uncertainty and variability. We have had only limited success (to date) at modeling differences between device responses based on characterization of their doping profiles. Furthermore, we have device characterization data (SIMS, SRP, construction analysis) on only 1 device for each type of analysis.

Because of these data limitations we have tried to utilize some of the information provided by the pre-rad gummel tests in estimating device performance. Figure 3 gives a scatter plot comparing the pre-rad inverse gain evaluated at base-emitter voltage .55 V compared with irradiated or "shot" inverse gain at time $t = 1$ sec. The base-emitter voltage .55 V is thought to be an appropriate point for distinction between the pre-rad performance of the devices. This plot (and those from some of the other experimental series) suggest a possible linear relationship between these variables. In the "Variability and Uncertainty Assessment" Section, we make use of this pre-rad data in the characterization of variability and uncertainty.

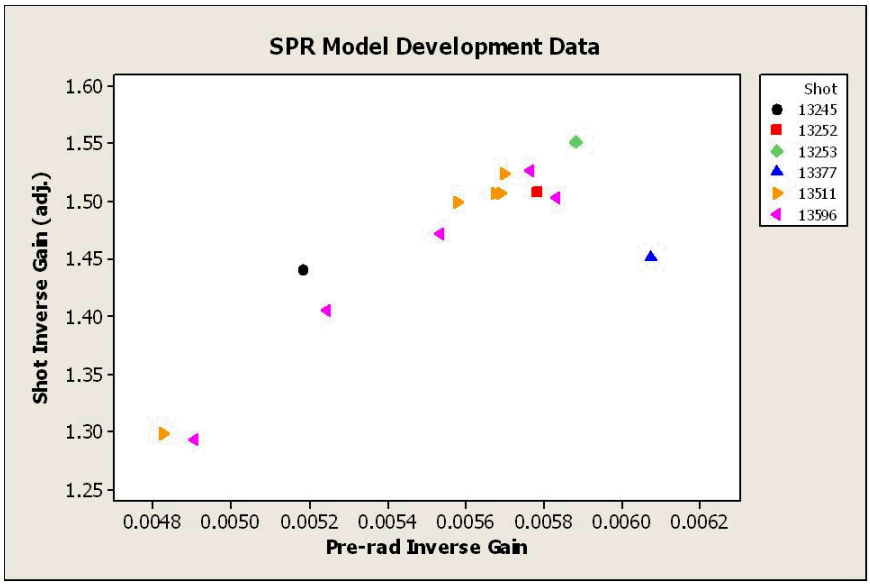

Figure 3. Scatter Plot Comparison of Pre-Rad and (Fluence Adjusted) Shot Inverse Gain

Facility and Device Bias Estimation

The uncertainty quantification and bias estimation process proceeds in steps where each step involves the analysis of data from an additional experimental shot series. The four data sets involved are used for the following purposes:

SPR Microsemi --	calibration;
ACRR Microsemi --	estimation of facility bias;
ACRR Fairchild --	estimation of device bias; and
SPR Fairchild --	comparison with model predictions.

Steps using the first three data sets are outlined in the "Calibration and Bias Estimation" Section.

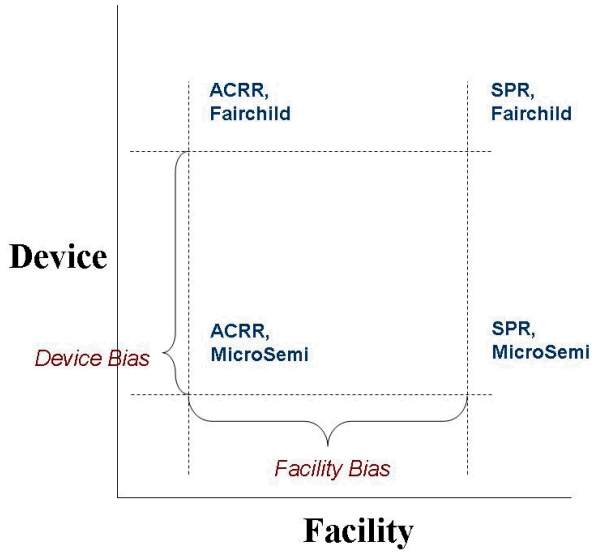

Figure 4. Two-dimensional Space Used for Calibration and Estimation of Device and Facility Biases.

Figure 4 gives a diagram of how this estimation and prediction process is accomplished. The facility bias is estimated comparing ACRR Microsemi results to SPR Microsemi results. The device bias is estimated comparing ACRR Fairchild results to ACRR Microsemi results. The methods used for model-based prediction in the SPR Fairchild quadrant of Figure 4 as well as those for a more general "threat" scenario are given in the "Model-Based Prediction" Section. Note that we have used the wording Fairchild and prototype and also Microsemi and model development synonymously to classified the devices throughout this report.

II Variability and Uncertainty Assessment

The analysis of SPR and ACRR shot data for the simple prototype analysis includes data from five separate experimental series. Inverse gain traces (normalized for fluence differences) for these data are plotted in Figure 5. The upper plot shows the only SPR data set used in this analysis. The middle two plots show ACRR shot responses for shots at relatively high fluence levels. The bottom plots show ACRR responses from shots at a lower fluence level. Note that the higher fluence ACRR shots yield responses that are more representative of the SPR responses. While the lower fluence data were used extensively in model development, the higher fluence shots have provided the basis for most of the simple prototype analysis.

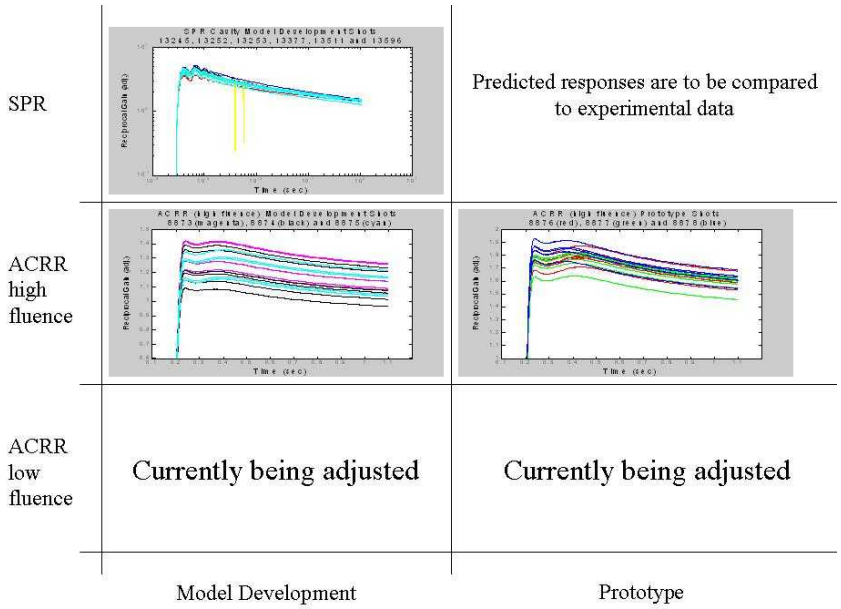

Figure 5. Inverse Gain Plots for the Five Experimental Data Series. **[ACRR low fluence shots are being re-normalized]**

Figure 6 shows scatter plots for the five data sets, comparing shot inverse gain at one second (vertical axis) to pre-rad inverse gain for the gummel C tests at base-emitter voltage .55 V (horizontal axis). These plots are scaled to cover the range of pre-rad testing (different for model development and prototype shots) and so that the vertical scale covers a range of about 25% of the mean response value.

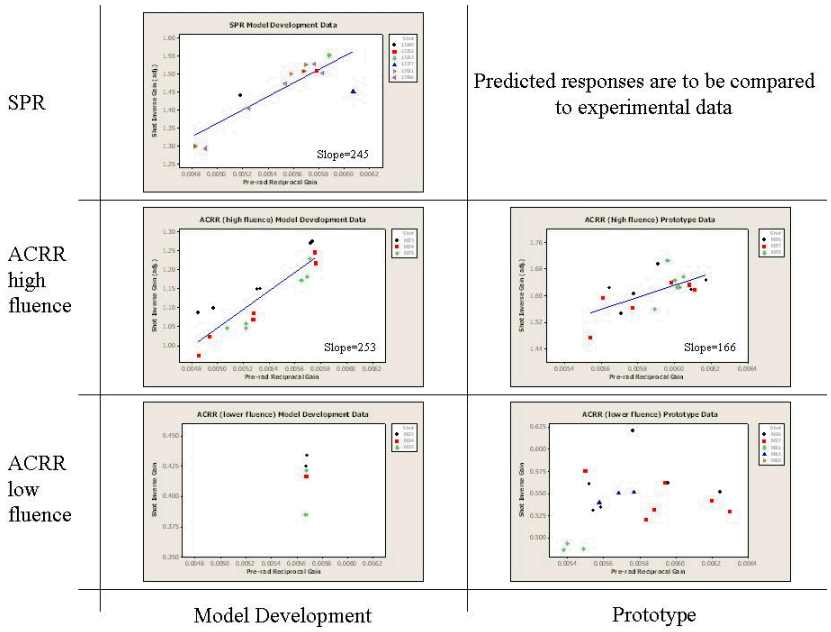

Figure 6. Scatter Plots Comparing Pre-Rad Inverse Gain to Inverse Gain for the Five Data Series.

Plots for the high-fluence ACRR shots and for the SPR microsemi shots show an indication of a trend or linear relationship between pre-rad and inverse gain performance. Statistical testing indicated that these trends are significant. Trends for the data sets shown in the lower two plots were not significant, however. The scales in pre-rad response was quite restrictive for the model development data limiting the ability to make inferences. It is puzzling, however, that the lower fluence ACRR prototype data set shows no trend. One possibility is that the facility uncertainty is dominant at these lower fluence levels, however, even for devices irradiated in the same shot there is no evidence of a relationship.

Given that a linear relationship exists for the higher fluence shots, it can be exploited to improve estimates of facility uncertainty and device uncertainty and variability in terms of both accuracy and precision. All pre-rad information can be used in the calculation of device variability providing a more precise estimate. Data from specific shots can also be adjusted to compensate for device differences where devices used in the shot are not "representative" in terms of their pre-rad performance. In general (but not always), this later adjustment has the effect of reducing the estimate for facility uncertainty.

Figures 7, 8 and 9 use the high-fluence ACRR prototype data to show more detail. We use these illustrations to describe the process used for calculating variability and uncertainty. The same process has been employed for each of the higher fluence experimental data series. The results are summarized in Table 2.

Table 2. Standard Deviation Table Standard Deviations after Adjustment for Pre-Rad Information.

Experimental Series	Mean, inverse gain	Device Variability (std. dev.)	Device Uncertainty (std. dev.)	Facility Uncertainty (std. dev.)
SPR Model Development	1.46	.073	.004	.076
ACRR (high fluence) Model Development	1.13	.077	.005	.049
ACRR (high fluence) Prototype	1.62	.052	.015	.022

The estimates in Table 2 are based on the data and statistical model:

$$r_{ij} = a + b(x_{ij}) + S_i + \varepsilon_{ij} \qquad (1)$$

Where:

r_{ij} is the inverse gain for the j^{th} device in shot i;

x_{ij} is the pre-rad inverse gain for this device and shot;
a and b are the parameters of the linear regression model;
S_i is the relative "effect" of the i^{th} shot (assumed to be based on the error in measurement of the boundary conditions, particularly fluence); and
ε_{ij} is an "error term" that captures variability from a number of sources.

Contributions to the error term are thought to be mostly device related, such as the nonlinearities in the pre-rad inverse gain – "shot" inverse gain relationship and further relationships that might be captured through different gummel tests or gummel C tests at different voltages. It is possible that some of the contributors to the term ε_{ij} are facility related such as a positional (during the shot) bias "spatial variation" that differs between facilities. The next three subsections provide an outline covering the computations of device variability, device uncertainty and facility uncertainty.

Estimate for Device Variability

Variability in the device response is a consequence of physical differences in the structure of the transistors that result from random or systematic variation in the manufacturing process. Quantifying device variability is a major part of the characterization required to predict the range of responses for any given scenario. The characterizations for device variability, based on experimental data and those generated through computational analysis should be compared as part of the validation procedure in the simple prototype analysis.

Figure 7 shows the data and regression estimate for the ACRR prototype data. This data set is used to establish parameter values used to predict device variability for the SPR prototype data. A density function $g(x)$ (approximated in Figure 7 through the scaled histogram of all gummel C tests on the prototype devices) is drawn below the x-axis. An inverse gain density function, $h(x)$ (approximated through a scaled histogram) is shown immediately to the left of the y-axis. This later density is the result of a linear scale adjustment and shift of $g(x)$. It provides an approximation to the response probabilities for the prototype devices that can be attributed to the linear relationship with pre-rad performance. It is computed as: $h(r') = g(x')$ where $r' = \hat{a} + \hat{b}(x')$ with $\hat{a}$ and $\hat{b}$ the least squares estimates of the regression coefficients a and b in Equation (1). The residuals (difference in a vertical direction between the plotted values and the corresponding modeled value (color-coded by shot)) can be seen in Figure 7. The ensemble of these values provides an estimate of the distribution of the errors ε_{ij} in Equation (1). We assign the errors the density function $\eta(\varepsilon)$.

A density approximation $h^*(r)$ is constructed as a further adjustment to $h(y)$ to include all variability (that attributed to the linear relationship and otherwise) in the devices. This is accomplished by convolving $\eta(\varepsilon)$ with $h(r)$:

$$h^*(r) = h(r) \circ \eta(r) = \int_{-\infty}^{\infty} \eta(\varepsilon) h(r - \varepsilon) d\varepsilon .$$

The density $h^*(r)$ is indicated through the leftmost scaled histogram in Figure 7. The associated standard deviations are provided in column 3 of Table 2.

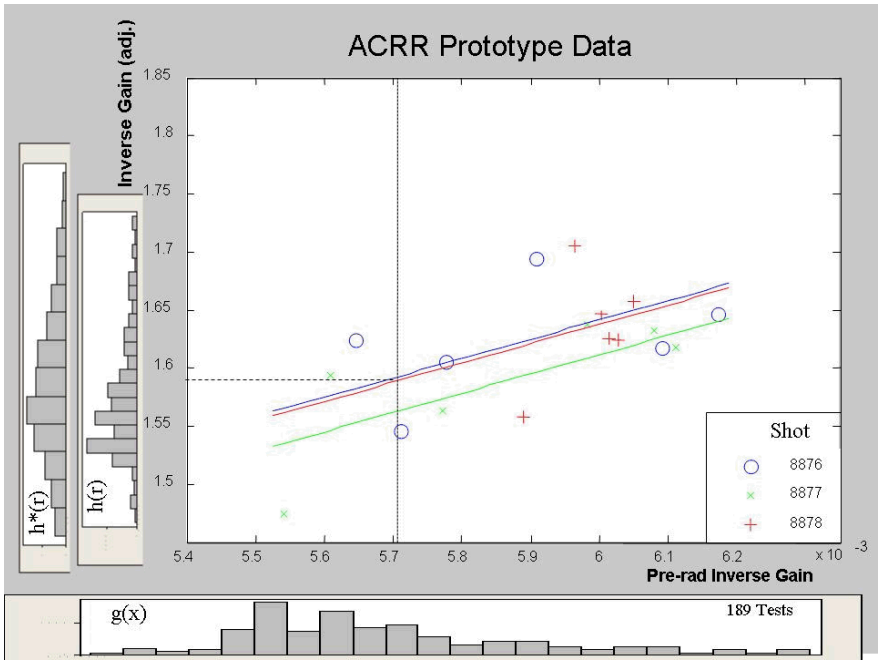

Figure 7. Plot Illustrating the ACRR Prototype Data and the Statistical Model in Equation 1 Fit to These Data.

Estimation of Device Uncertainty

Device uncertainty refers to uncertainty in the inverse gain mean because of data limitations. We use uncertainty in the mean estimates to calculate uncertainty in the device bias estimate. Figure 4 indicated, roughly, how the device bias is obtained. It is based on estimates of the device mean for both ACRR data sets. In this subsection, we focus on the ACRR (high fluence) prototype data series and show the calculation for uncertainty in the inverse gain mean value.

Note from Figure 7 that the distribution of the pre-rad inverse gain is based on 189 gummel C tests. It is reasonable to assume that the mean value is close to the computed value 5.706. There is still substantial uncertainty in the inverse gain mean, however, as a consequence of limited data (18 devices three shots with six devices each) used for the regression calculations. Figure 8 shows how uncertainty in the linear regression coefficients $\hat{a}$ and $\hat{b}$ leads to uncertainty in the inverse gain mean. The curved lines indicate 95% (pointwise) confidence bounds for the regression line $a + bx$ under the typical assumptions of regression analysis (see "Regression Analysis by Example" Chatterjee and Price (1977)). These should be close to "2-sigma" bounds (two standard deviation on either side of the regression line). The vertical line corresponds to the pre-rad inverse gain mean for all Fairchild devices tested. The horizontal lines intersecting the bounds show how these bounds can be used to infer uncertainty for the inverse gain

mean. These lines indicate the range of (approximately) 2-sigma bounds on the inverse gain mean corresponding to 5.706 volts. The standard deviations calculated using these bounds are provided in the fourth column of Table 2.

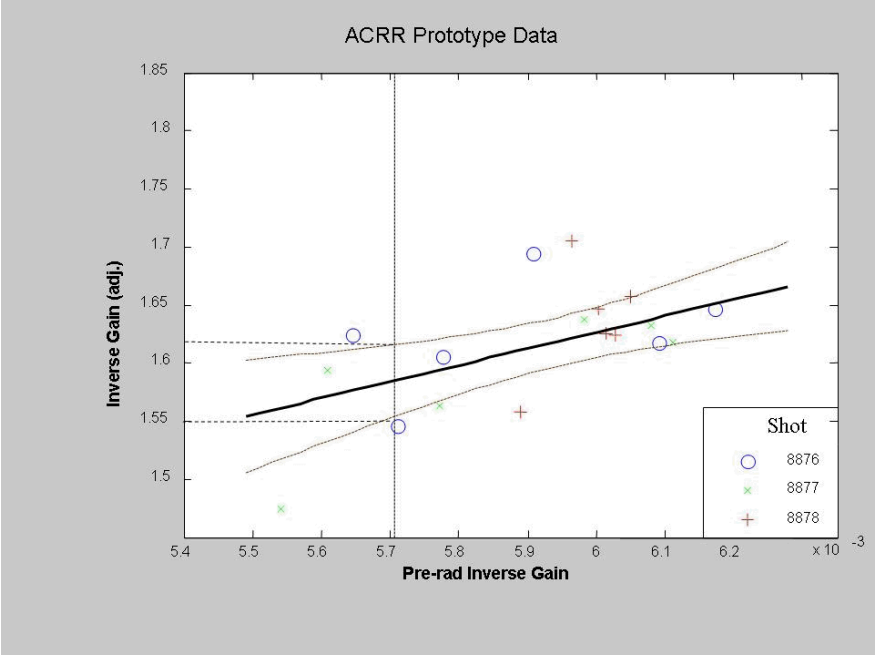

Figure 8. Plot Illustrating the Process of Estimating Uncertainty in the Inverse Gain Mean.

Estimation of Facility Uncertainty

Facility uncertainty refers to the response differences that result from uncertainty in the boundary conditions associated with each shot and each device. Facility uncertainty is dominated by random errors in specification of fluence levels associated with the shots. Figure 9 shows again the ACRR prototype data and regression calculations. In this subsection we use these data to indicate how the estimate of facility uncertainty is calculated including an adjustment to accommodate shot-to-shot differences in the pre-rad device levels.

Note that three separate regression lines are provided -- one for each shot. The separate regression lines are an indication of the difference between shot means (adjusted for differences in pre-rad device performance). The colored boxes in Figure 9 indicate the mean values for pre-rad and shot inverse gain for each shot. Differences in the pre-rad level compared with the pre-rad mean show a selection bias associated with each shot. One can draw a vertical line at the mean pre-rad level and shift the shot means along the associated a regression lines to meet at this line. This has the effect of adjusting the inverse gain shot means for pre-rad bias. Estimating the uncertainty in inverse gain where these shifted mean values meet the vertical line gives an "adjusted" estimate for the terms S_i. The value S_i is computed as the i^{th} value indicated by the horizontal line minus the mean of the three values. The standard deviation in these adjusted shot

estimates is the major component of the facility uncertainty. There are other contributors. Uncertainty in the mean value based on the three shots and uncertainty in the shot average because of the limited number of devices per shot provide minor contributions. Note that these later components are treated differently for the computation of prediction uncertainty as described in the last subsection of this report. The values combined from these sources are listed in the fifth column of Table 2.

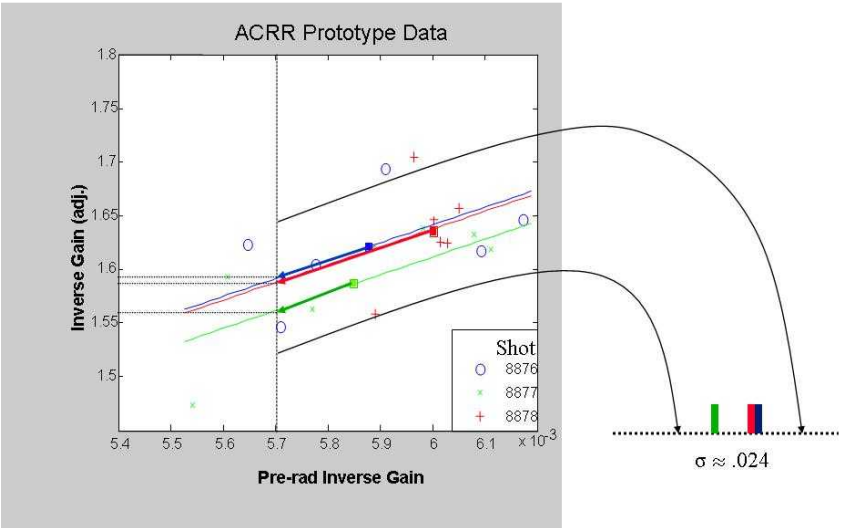

Figure 9. Shot Estimate Adjustment For Pre-Rad Device Bias.

III Calibration and Bias Estimation.

The approach used in predicting the SPR Fairchild response is to utilize ACRR experimental and computational results to estimate a "device bias" (Microsemi compared with Fairchild). This bias is then added to the SPR Microsemi mean response when making the Charon SPR Fairchild predictions. In implementing this process, it is necessary to first estimate a "facility bias" (SPR compared with ACRR Microsemi responses). Adjustments to accommodate these biases are made on the computational side through multipliers applied to either the Frenkel Pair multiplier (facility bias) or the X-section multiplier (device bias).

We feel the steps in this analyses are most easily explained in "multiplier space" shown in Figure 10. Each step is shown through developments in one "quadrant" of the space. The quadrants are labeled in Figure 10, and notation is introduced for the multipliers used in the analysis. The subscripts represent: S – SPR; A – ACRR; M – Model Development (Microsemi); and P– Prototype (Fairchild). Note that most of this analysis can be (and was) performed in terms of inverse gain. It is required, however, that the multipliers be established to make the model predictions. More detail is provided in Appendix B.

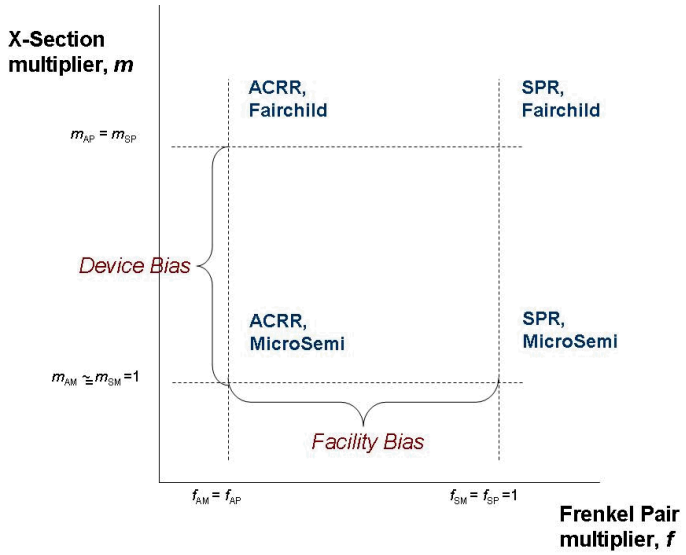

Figure 10. Multiplier Space Representation of the Calibration, Bias Estimation and prediction Processes.

Calibration.

The calibration process involved the number of steps with several physics parameters (see "Prototyping the QASPR Simple Prototype Exercise", W.R.Wampler 1/18/2008 for details). The discussion in this subsection provides a simplification of the process that should be sufficient for our objectives. The calibration step involves experimental data from the SPR Microsemi shots. First, the X-section multiplier m_{SM} is normalized to 1 (that is, values for this parameter are established at their current values and the multiplier is set to 1). Next an inverse-problem approach (see Appendix A) was utilized to find the Frenkel Pair multiplier f_{SM} that generate a Charon response that provides a close approximation to the response for each shot. The average value is normalized so that the Frenkel Pair multiplier is 1. While the average value of these multipliers is set to one, there range provides a basis for facility uncertainty quantification in the computational analysis. The individual shot response estimates for the SPR Microsemi shots and the corresponding multipliers are listed in Table B1 in Appendix B.

Figure 11 illustrates this process in a rough fashion. The density functions and symbols indicating where the shot data are plotted is not drawn to scale of the bias estimates. The vertical bars in the SPR Microsemi quadrant (they are drawn by hand in Figures 11, 12 and 13) indicate the values of the Frenkel Pair multiplier calculated for the 6 shots; the horizontal density (scale is arbitrary) indicates the distribution of values calculated for the X-section multiplier by applying the inverse procedure (Appendix A) to points of the inverse gain distribution established for device variability of the SPR Microsemi data. The blue circle in the SPR Microsemi quadrant indicates the device uncertainty (vertically) and the component of facility uncertainty (horizontally) that comes from uncertainty in the shot mean value due to its estimation, based on only six shots. It should be emphasized again here that no scale is provided the Figures 11 through 13, as they are used only as an aid in describing the process. A more detailed description of

"calibration uncertainty" is given in Appendix B. In the next two sections, this process is repeated using ACRR data estimating the Frenkel Pair multiplier (using ACRR model development data) and the X-section multiplier (using ACRR prototype data). The differences between the estimated multiplier mean values and the calibrated values (1's) are used to approximate the facility and device bias estimates respectively.

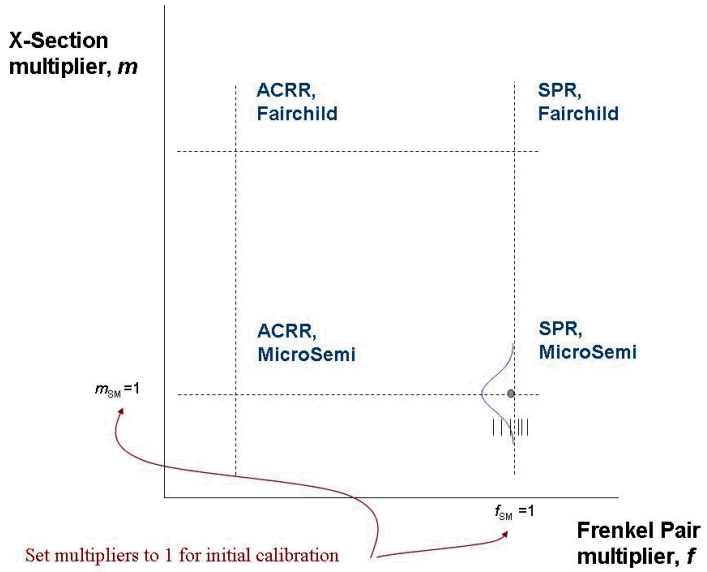

Figure 11. The Calibration Process in Multiplier Space.

Estimating the Facility Bias

The data analysis process outlined in the previous sub-section was applied to the ACRR Microsemi data. Summary results are listed in Table 2 and illustrated in Figure 12. The shot response estimates are, again, the fluence adjusted inverse gain estimates at time t = 1 second. The Frenkel Pair multiplier values listed in Table B1 are the result of applying the inverse procedure to each shot. These f values form the vertical bars (drawn by hand) in the ACRR Microsemi quadrant of Figure 12. The horizontal density indicates a distribution of values calculated for the X-section multiplier by applying the inverse procedure to percentiles of the distribution of inverse gain values established for the ACRR Microsemi data. The shot average Frenkel Pair multiplier is .88 -- indicating a "facility bias" at ACRR of .88 – 1 = -.12 expressed as a unitless multiplier of the Frenkel Pair parameter. The shot average X-section multiplier was maintained at value 1. The uncertainty associated with the facility bias estimate is computed in Appendix B.

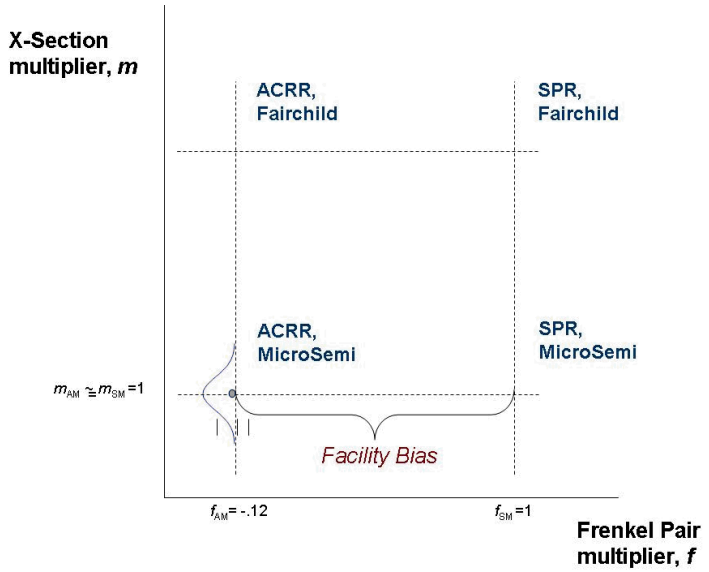

Figure 12. Estimating the Facility Bias in Multiplier Space.

Estimating the Device Bias

The data analysis process outlined in the calibration section was applied to the ACRR Fairchild data. The results are listed in Table 2 and illustrated in Figure 13. The Frenkel Pair multiplier values listed in Table B1 are the result of applying the inverse procedure to each shot. These *f* values are indicated through the vertical bars drawn in the ACRR Fairchild quadrant of Figure 13. The horizontal density indicates the distribution of values calculated for the X-section multiplier by applying the inverse procedure to values from the distribution of inverse gain established for device variability of the ACRR Fairchild data. Variability established using this density function is used to estimate the device variability for the SPR Fairchild predictions. The shot average X-section multiplier is 1.07 -- indicating an estimated device bias at ACRR of 1.07 - 1 = .07 expressed as a unitless multiplier of the X-section parameter. The uncertainty associated with the bias estimate is computed in Appendix B.

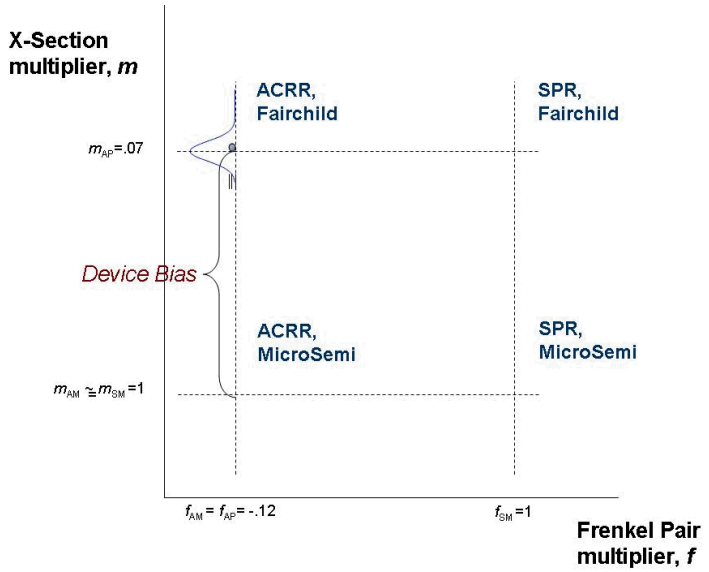

Figure 13. Estimating the Device Bias in Multiplier Space.

IV Model-based Prediction

In the previous section we explained how, through tests at ACRR, we are able to estimate a device bias that we now apply to SPR and more general predictions for the Fairchild devices. We also characterized variability and uncertainty for these predictions through the X-section and Frenkel Pair multipliers. These characterizations are carried forward to estimate uncertainty in the predictions described in this section.

Predictions for the SPR Fairchild data.

Predictions for the SPR Fairchild data are made by using the Charon predicted response with boundary conditions matching those in the SPR Fairchild shot series and adjusting the X-section parameter by multiplying by 1.07 (the estimated device bias). Figure 14 illustrates this final step in the analysis. Uncertainty and variability associated with the prediction are indicated by the rectangle and the ellipse in the SPR Fairchild quadrant of the figure. The rectangle indicates bounds based on the facility uncertainty from the circled area in the SPR Microsemi quadrant and the device variability from the circled area in the ACRR Fairchild quadrant. The center ellipse in the SPR Fairchild quadrant represents uncertainty based in limitations on the data. The uncertainty is greater in the vertical (device) direction reflecting uncertainties in both ACRR data sets used to calculate the device bias, as well as in the SPR Microsemi mean value to which the device bias is added. Uncertainty in the facility mean comes from the SPR Microsemi data and is the result of data limitations there. The red "+" symbols represent points in multiplier space corresponding to 2-sigma bounds on the distributions formed as the convolution of densities that generated the bounds indicated by the rectangles, and the ellipse. These are used here as in Figure 1a to construct prediction bounds for the evaluation of QASPR prediction capabilities.

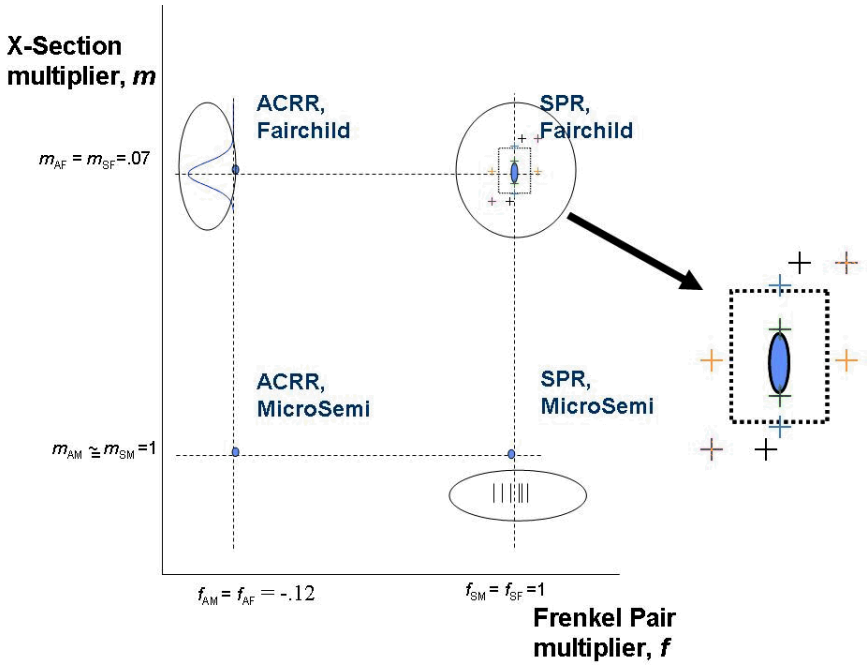

Figure 14. Predictions in Multiplier Space.

Using multiplier values computed to produce proximate 95% bounds, together with specified boundary conditions matching a particular shot and device from the SPR prototype series, Charon runs were used to generate bounds like those in Figure 15. These bounds can be compared to the experimental data for corresponding shot and device. We are able to compute bounds for the predicted response with only two runs of the computational model because the inverse gain response changes are monotonically increasing with both multipliers, (multipliers are indicated by the red "+" symbols in Figure 14).

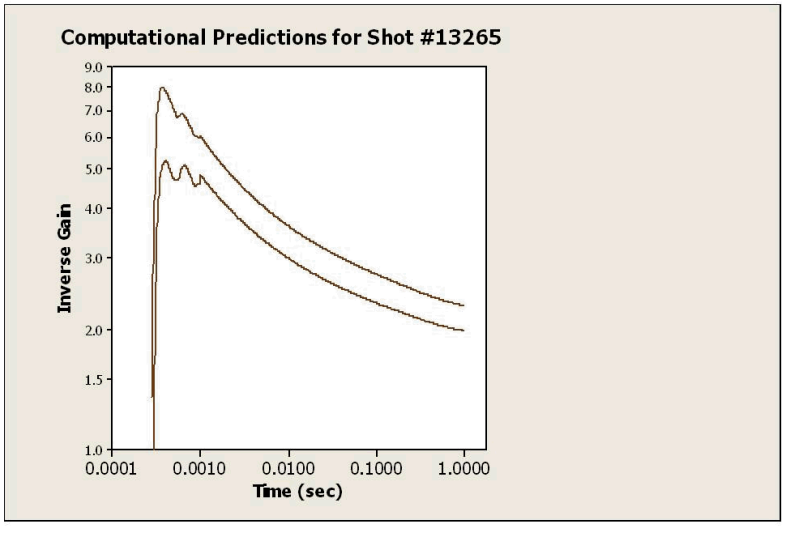

Figure 15. Computational Bounds Computed for Simple Prototype Shot #13265.

In addition to the bounds computed for each shot and device, the QASPR characterizations for variability and uncertainty should be compared to experimental data. These variability and uncertainty estimates are maintained through distributions or bounds on the multiplier values. Computational runs using nominal boundary conditions and multiplier values indicated by the blue "+"s at the top and bottom border of the rectangle yield bounds on device variability. Computational runs using multipliers indicated by the gold "+"s to the left and right of the rectangle indicate bounds on facility uncertainty and computational runs indicated by the green '+'s above and below the ellipse provide bounds for device uncertainty. These quantities should be compared to values computed from the SPR prototype data using the process described in Section II.

Predictions for a General Threat Environment.

For the threat environment or for any predictive scenario were boundary conditions are specified (without uncertainty), only a small portion of the facility uncertainty is applicable -- the portion that quantifies uncertainty in the mean value for the 6 SPR Microsemi shots (indicated through the width of the ellipse). This quantity represents uncertainty in the inverse gain value used in calibration for normalization to the Frenkel Pair multiplier value 1. Values of the multipliers used for the computation are indicated in Figure 14 by the black "+" symbols above and below the rectangle in the SPR prototype quadrant. Again, by making use of the fact that response is monotonic to changes in the X-section multiplier, bounds on the prediction can be established through only two computational runs.